Available online at www.sciencedirect.com

ScienceDirect

Energy Procedia 114 (2017) 4008 – 4019

Energy Procedia

13th International Conference on Greenhouse Gas Control Technologies, GHGT-13, 14-18 November 2016, Lausanne, Switzerland

Assessment of the limitations on the seismic detectability of injected CO_2 within a deep geological reservoir

Lisa A. N. Roach[a]*, Doug A. Angus[a], Don J. White[b]

[a]*University of Leeds, Leeds, LS2 9JT, United Kingdom*
[b]*Geological Survey of Canada,Ottawa, K1A 0E8 ,Canada*

Abstract

Aquistore is a deep saline CO_2 storage research and demonstration project located near Estevan, Saskatchewan where CO_2 is transported via pipeline and injected into a sandstone reservoir ~3200 m below the surface. A pre-injection time-lapse analysis performed on two sparse 3D seismic datasets was used to characterise the background time-lapse signal-to-noise level at the storage site. The time-lapse analysis revealed that the lowest global nRMS was 0.07 which was taken to represent the level above which CO_2 would be detectable in the reservoir. We investigate the conditions under which the injected CO_2 can be detected above the defined minimum noise level through Gassmann fluid substitution and 3D seismic forward modelling. Additionally, Wave Unix was used to simulate the seismic response of the reservoir due to the injected CO_2 by generating the synthetic surface reflection seismic data from an explosive surface P-wave source. We generated noise-free synthetic seismograms for the baseline model as well as for the 2-phase fluid replacement of brine with CO_2 for CO_2 concentrations up to 100% within the target zone – the monitors. The baseline and monitor traces from the 3D seismic survey at Aquistore are used as the noise traces in this study, and were added to their respective baseline and monitor synthetic traces. The nRMS within the reservoir was then computed for the noisy baseline and various noisy monitor surveys and was used in the assessment of the limitation to the detection of the injected CO_2 in the reservoir under the background noise level at the site. We are able to conclude that the time-lapse repeatability will not limit the ability to monitor the CO_2 induced changes in the reservoir at the Aquistore storage site.

Peer-review under responsibility of the organizing committee of GHGT-13.

Keywords: CO_2 storage; 4D; time-lapse seismic; noise, fluid replacement modelling; Aquistore

* Corresponding author. Tel.: +44(0)-113-343-5543; fax: +44(0)-113-343-5259.
E-mail address: l.a.n.roach@leeds.ac.uk

Peer-review under responsibility of the organizing committee of GHGT-13.
doi:10.1016/j.egypro.2017.03.1541

1. Introduction

The capture and sequestration of CO_2 is expected to contribute significantly to the management of greenhouse gas emissions. One of the options for the geological storage of CO_2 in the mitigation of climate change is its injection into deep saline aquifers. Located in Saskatchewan, Canada, Aquistore is one of the global projects aimed at demonstrating the safety of deep saline formations for the geological storage for CO_2. At the Aquistore site, CO_2 will be pipelined from the SaskPower's Boundary Dam power station and injected into the saline aquifer sandstone reservoir at a depth of approximately 3200m – 3350m that has thick and laterally extensive shales acting as its primary seal.

The major objective of CO_2 monitoring is the tracking of CO_2 that has been injected into the subsurface. Effective monitoring of CO_2 distribution relies on the ability to detect the CO_2 within the reservoir. The presence of CO_2 is expected to create a visible change in the magnitude of the seismic properties of the reservoir sediments. These changes are captured in the amplitudes of the recorded seismic data and can be used to assess the ability to detect, and thus monitor the presence of the injected CO_2. Time-lapse seismic surveying has been successfully employed for CO_2 reservoir monitoring to track changes in the subsurface over time due to the presence of CO_2 [1,2,3,4] The time-lapse noise level, however, is one of the factors that influences the ability to image the injected CO_2 [5]. The aim of this study is to evaluate the limit of CO_2 detectability at the storage site within the background noise level present.

Fluid substitution modelling is a tool that allows for investigating the influence of CO_2 on the physical rock properties. Biot-Gassmann fluid substitution [6,7] was used to estimate the changes in p-wave velocity, s-wave velocity and density of the reservoir rock towards determining the extent and conditions under which CO_2, when injected into the reservoir, is detectable by the Aquistore permanent array under the time-lapse noise conditions.

The reservoir consists of the Winnipeg and Deadwood Formations which is bounded by the Yeoman at the top and by the Precambrian at the bottom. Results from drill-core analysis were used to delineate the rock types in the target formation for the purpose of modelling. This resulted in the reservoir being subdivided into four units based on rock type and were modelled as three zones to account for various fluid movement scenarios in one instance and as a single block in another.

The normalized root mean square (nRMS, [8]) is the metric employed for quantifying the amplitude differences between the baseline and monitor traces. The nRMS as a fraction is defined as

$$nRMS = \frac{2\sqrt{\sum_{t_1}^{t_2}(b_t - m_t)^2 / N}}{\sqrt{\sum_{t_1}^{t_2}(b_t)^2 / N} + \sqrt{\sum_{t_1}^{t_2}(m_t)^2 / N}} \quad (1)$$

where b is the baseline trace, m is the monitor trace. The RMS is computed within a given window t (t_1-t_2, with start and end times of t_1 and t_2, respectively) and N represents the total number of samples per trace within the window. nRMS values range from 0 to 2, where the values decrease with increasing repeatability between traces. When the nRMS is computed for the entire dataset, it is referred to as the global nRMS (GnRMS).

2. Model creation and synthetics generation

Gassmann fluid replacement modelling was used to estimate the changes in the reservoir rock properties as a result of replacing brine with CO_2 in the sediments. Specifically, Gassmann was used to estimate the changes in the P-wave velocity, S-wave velocity and density of the reservoir due to the presence of various concentrations of CO_2 in the pore space at the approximate salinity, pressure and temperature of the target zone. The initial geological model, which represents the baseline of the geological sequence, was derived from the well-log data collected at the Aquistore injection well (UWI 101050600208W200) prior to CO_2 injection. Table 1 lists the rock properties of this simplified geological model. The s-wave velocity log was generated using *in situ* p-wave and density logs as input into Castagna's [9] relationship. The rock-matrix densities were derived from the weighted average of the mineral components obtained from the well logs, and the moduli from averaging of the mineral moduli. Batzle and Wang [10]

was used to determine the properties of the brine at 120°C, 35Mpa and 300,000 ppm, respectively. Table 2 details the rock properties within the target zones, their segmentation, and the modelling parameters.

Table 1. Simplified geological model for modelling the fluid replacement response within reservoir. The red box outlines the rock properties of the three zones which are averaged for the single layer reservoir model.

Layer	Rock Type	Thick. (m)	Vp (m/s)	Vs (m/s)	ρ (kg/m^3)
Modelling	-	670	2567	1500	2100
Modelling	Shale	451	2637	1512	2390
Modelling	Sandstone	356	3437	2104	2479
Watrous	Anhydrite	127	4352	2420	2610
Poplar	Dolomite	488	5643	3029	2700
Bakken	Shale	30	4379	2522	2510
Torquay	Anhydrite	59	4703	2655	2665
Birdbear	Limestone	329	5854	3127	2737
Prairie Evaporite	Salt	155	4456	2482	2067
Ashern	Dolomite	295	6271	3333	2759
Layer	Limestone	165	6121	3286	2745
Winnipeg Ice Box	Shale	24	4474	2430	2696
zone 1	Sandstone	49	4802	3010	2600
zone 2	Limestone	95	4988	2840	2644
zone 3	Sandstone	49	4858	3015	2583
Precambrian	Quartz	---	5579	3203	2638

Table 2: Characteristics of the reservoir rocks.

Unit	Zone	General rock type	Avg. rock matrix mineral composition (%)				Thickness (m)	Avg. φ (%)
			Calcite	Dolomite	Illite*	Quartz		
Winnipeg Black Island	1	SS	1.6	0.89	12.1	78.8	44	6.6
Deadwood		SS	31.3	8.12	19.6	37.5	32	2.9
Deadwood 1	2	LS	6.3	2.22	33.5	50.1	68	6.2
Deadwood 2	3	SS	2.1	0.4	15.5	75.12	49	7.4

*modelled as muscovite. SS – sandstone, LS – limestone.

Fig. 1 shows the p-wave velocity, s-wave velocity and densities of the reservoir region before and after CO_2 substitution and the change in these properties as a function of CO_2 saturation. A 2-phase fluid substitution modelling method was used where brine was replaced with CO_2 in saturations of 5% increments up to 100%. These models with different CO_2 concentrations are considered the synthetic monitor models.

The evaluation on impact of noise on the ability to detect CO_2 in the reservoir was investigated through two approaches: (i) a thickness-CO_2 saturation model; and (ii) a single-zone model. The thickness-CO_2 saturation approach included CO_2 distribution through the varying of the thickness of the CO_2 filled layer within the reservoir using a top-down method. This top-down method is based on the assumption of the upward migration of CO_2 to the top of the reservoir to fill the un-saturated regions up to the point of saturation. The thickness of the layer was varied in 1m increments up to 100% of the zone thickness. For the single-zone approach, on the other hand, the reservoir is treated as single 193 m thick layer where CO_2 replacement is within the entire layer. Here, there were 6 different CO_2 saturations: 0 %, 5 %, 10 %, 20 %, 30 %, 50 % and 100 %.

In both approaches, the baseline dataset is represented by a 100% brine saturation (i.e. 0% CO_2 saturation).

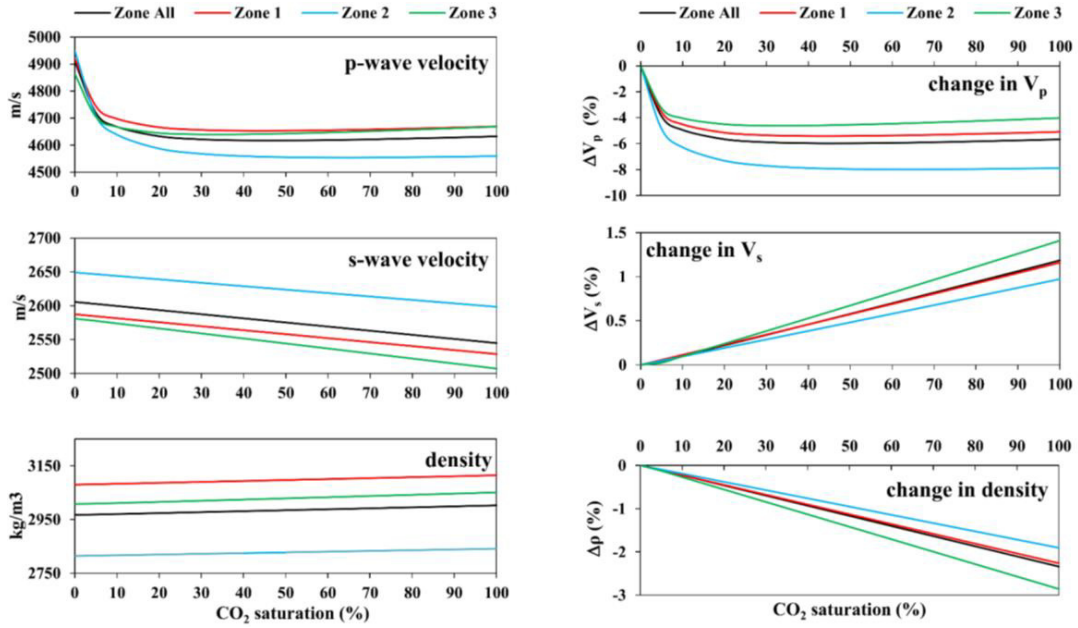

Fig. 1: (Left) p-wave and s-wave velocities and density as a function of CO_2 saturation for each zone. (Right) Changes in density and p-wave and s-wave velocities with CO_2 saturation for each zone. The curves represent the entire interval of each zone being saturated with a constant CO_2 saturation.

For the thickness-CO_2 saturation models, the seismic response of the sediments to the presence of CO_2 in the pore space was simulated by 1D seismic forward modelling resulting in nmo-corrected synthetic CDPs for each of the thickness-CO_2 saturation scenarios, for each of the zones. Each of the layer-thickness-CO_2 saturation scenarios are a proxy for the monitor datasets.

For the single-zone approach, a suite of 14-layer data models was created to be used in the generation of synthetic surface reflection seismograms. For the suite of models, the p-wave, s-wave and density for the reservoir region (the average of the properties of zones 1, 2 and 3 in Table 1) were determined for the various CO_2 saturations. The models with CO_2 filled layers are referred to as the monitors.

The synthetic surface reflection seismic data were generated using the anisotropic finite difference software, Wave Unix [11], which produces primary reflections, multiples and P-S and S-P converted waves. A surface P-wave source was used and Aquistore's data acquisition geometry [12] was replicated. Due to time-constraints, 25 synthetics shotgathers were created from 25 shots 'fired' into 630 receivers instead of the full complement of 260 shots used in the acquisition of the real data. Fig. 2 shows the shot-receiver locations of the synthetic dataset.

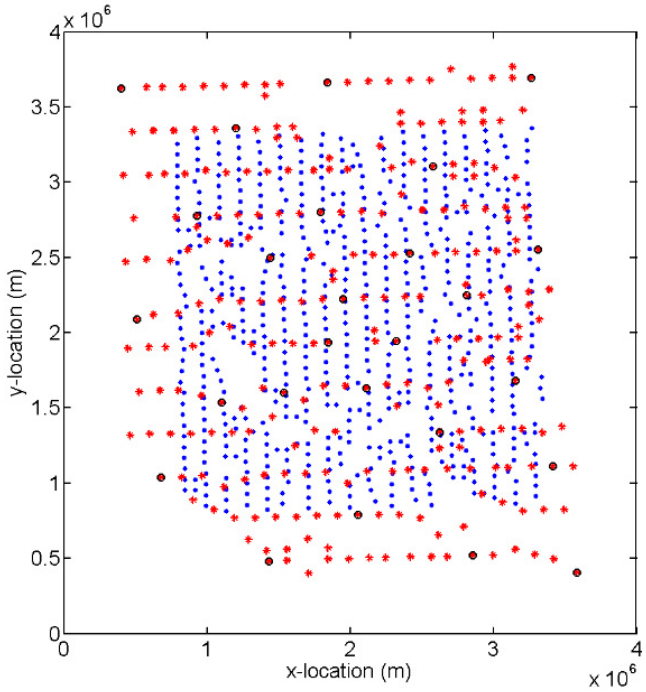

Fig. 2: Shot-receiver locations for the Wave Unix single-zone synthetic data generation. Blue dots are the 630 receiver locations, red stars represent the 260 shot locations and the black circles pinpoint the subset of 25 shots used in generating the synthetic data.

3. Noise traces

Roach et al. [12] conducted a pre-CO_2-injection time-lapse analysis using two 3D dynamite seismic surveys to assess and characterize the background time-lapse signal-to-noise level for the areal permanent array data at the Aquistore CO_2 storage site. These seismic datasets were acquired at the storage site in 2012 (baseline) and 2013 (monitor) using a permanent sparse array, so called because it has much fewer receiver-shot pairs than a commercial scale 3D acquisition. White et al. [13] have provided evidence for and the justification of the permanent array while in the companion paper, Roach et al. [12] demonstrated that the repeatability between the pre-injection surveys is well below that ever achieved by other surveys. The full processing flow included a 4-step post-stack cross-equalisation sequence after which the similarity between the pre-injection baseline and monitor volumes was large – a global nRMS value of 0.07 over the entire coherent volume – from 700ms down to the Precambrian basement at 2000ms. The global nRMS of 0.07 within this time window defines the time-lapse background noise level at the Aquistore CO_2 storage site and was taken to be the threshold noise-level above which changes in the CO_2 concentration would be detectable within the reservoir.

The way the baseline and monitor 3D dynamite seismic survey traces were used as noise was dependent on the investigative approach. For the thickness-CO_2 saturation models, the noise traces are the real baseline and monitor traces with the minimum residual seismic amplitudes differences, i.e. the set of stacked baseline and monitor traces from the real volumes after the final step in the cross-equalisation process. Thus, the cross-equalised post-stack traces of the monitor volume were used as the monitor noise and the baseline migrated traces were used as the baseline noise traces for this set of models. In this instance, the 0.07 global nRMS values represents the threshold noise level.

For the single-zone reservoir approach, the raw real baseline and raw real monitor traces were used as the noise traces. Here, the threshold noise-level is defined as the global nRMS of the completely processed subset of noise traces (after the final cross-equalisation step (PTSN (see figure 12)) within the reservoir region.

4. Data processing

The cross-equalised pre-injection volumes consisted of 6475 stacked traces with trace-by-trace nRMS values ranging from 0.01 to 0.7[12]. Therefore, a subset of these cross-equalised traces needed to be selected to be added to the thickness-CO_2 saturation synthetic traces which are also stacked traces. The first selection criterion imposed was that only those cross-equalised traces with nRMS values between 0.065 and 0.07, computed within the window 700ms to 2000ms, were used as the noise traces. For further reduction of the number of noise traces to compliment the number of synthetic traces, an additional criterion was used – the trace-by-trace nRMS computed within the window corresponding to the zone's thickness must be around 0.1 (the global nRMS of traces within the reservoir window of each zone). The background time-lapse noise threshold is then compared to the calculated seismic responses to determine the likelihood that 4D seismic data will be capable of detecting CO_2 in the deep saline aquifer at the Aquistore site.

For the single-zone approach, the subset of shot-receiver raw real trace pairs that corresponds to the synthetic shot-receiver traces were selected and summed to the synthetic traces. The trace-by-trace nRMS for the subset of 14,235 raw (un-stacked) traces (compared to the ~153,000 traces in the real time-lapse analysis) ranged from 0.14 to 1.77 for the large-window and 0.02 to 2.0 for the reservoir. The raw synthetic dataset with noise added was then processed using the '4D-friendly simultaneous' processing steps outlined in Roach et al. [12] which included a standard pre-stack processing sequence and a post-stack cross-equalisation sequence.

Additionally, the subset of raw noise traces were also processed using the 4D-friendly simultaneous processing sequence for direct comparison with the noisy synthetic datasets. After the application of each processing step, stacks were created of the noisy synthetics and of the noise traces. Data repeatability was tracked along the stages of the time-lapse processing through the computation of the nRMS on the stacked volumes after each processing step. The nRMS was also computed for the reservoir region at each CO_2 saturation on the cross-equalised volume and compared to the nRMS of the cross-equalised noise traces to determine the potential of detecting CO_2 at the storage site.

In both the thickness-CO_2 saturation and single-zone approaches, the noise traces need to be scaled before they were added to the synthetics. The trace-by-trace scaling factor applied was defined as the ratio of the RMS of the noise data traces to the RMS of the synthetic data traces. The RMS was computed within the window 700 ms to 2000 ms.

5. Results

5.1. The thickness-CO_2 saturation models

Fig. 3 through to 7 summarise the results of the thickness-CO_2 saturation models. Fig. 3 shows the subset of monitor noise traces that were used as well as the nmo-corrected CDP stacked traces for zone 3 where each trace represents a CO_2 saturation – layer thickness scenario. In Fig. 4, which shows a close-up of the reservoir section of Fig. 3, a clear variation in the amplitude as a function of CO_2 saturation and thickness is seen – i.e. the amplitude of the signal increases with increasing CO_2 saturation and layer thickness, as expected.

Fig. 5 shows the baseline and monitor (100% CO_2 saturation) traces with their respective noise added as well as the amplitude differences between these noisy baseline and monitor traces for zone 3. The panels of the noisy baseline and monitor traces serves to demonstrate the complete obscurity of the CO_2 signal in the traces after the addition of noise. However, an anomalous amplitude above the noise is visible in the difference sections within the region in which an amplitude difference is expected due to the presence of CO_2. This observation is valid for each of the zones (not pictured).

Fig. 6 compares the amplitude difference between the baseline traces and their corresponding monitor traces for each of the zones. Fig. 6A shows the noise-free differences while Fig. 6B shows the noisy differences. Again, the anomalous amplitudes is visible above the threshold noise for each of the CO_2 saturation – layer thickness scenarios.

In an effort to quantify the observed seismic amplitude differences between the monitor and respective baseline traces, the nRMS was computed for each layer-thickness-CO_2 saturation scenario. The nRMS for the noise-free and noisy traces are displayed, as a function of thickness and CO_2 concentration for each modelled zone, in Fig. 7.

Defining the minimum condition for CO_2 detection as the layer thickness and CO_2 saturation combination that results in the nRMS value greater than 10% results in the following observations: for the Winnipeg Ice Box to

Deadwood units (zone 1), the minimum condition for detecting CO_2 is met (or exceeded) when the CO_2 saturation is 5% within a 11m thick zone. For the Deadwood 1 unit (zone 2) CO_2 is detectable if the CO_2 saturation is at least 5% within a zone thicker than 5m. In the case of the Deadwood 2 unit (zone 3) , the minimum nRMS above the threshold occurs when the layer thickness is at least 5m and the CO_2 saturation is above 5%. A comparison with the noise-free results yields the similar the minimum conditions for CO_2 detection.

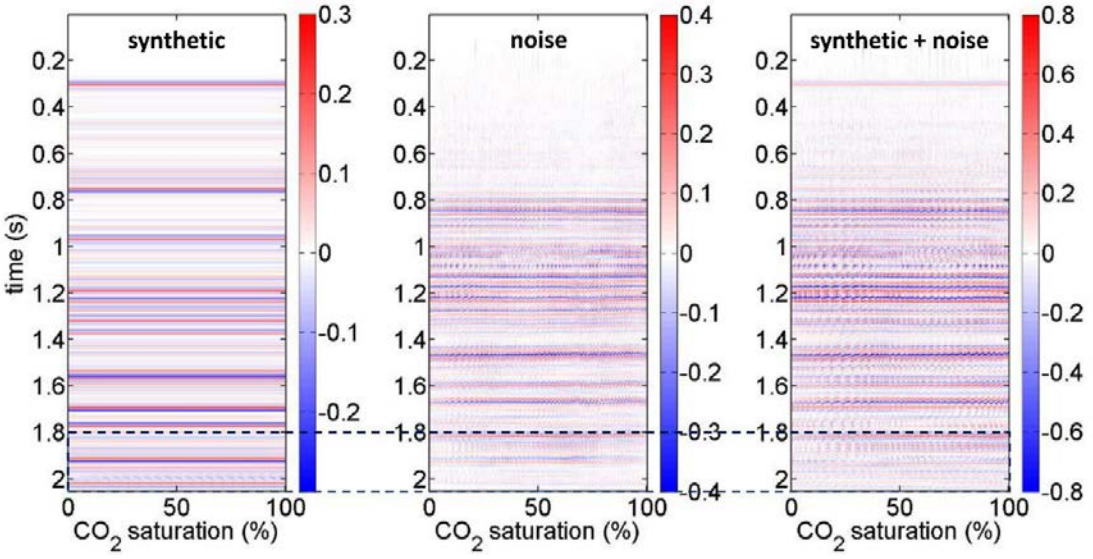

Fig. 3. Sample of the noise and synthetic traces. (Left) an example of the synthetic traces resulting from a CO_2 saturation of 100%, (middle) the monitor noise traces and (right) the sum of the noise and the synthetic traces. The blue dash lined outlines the reservoir region and is plotted in Fig.4.

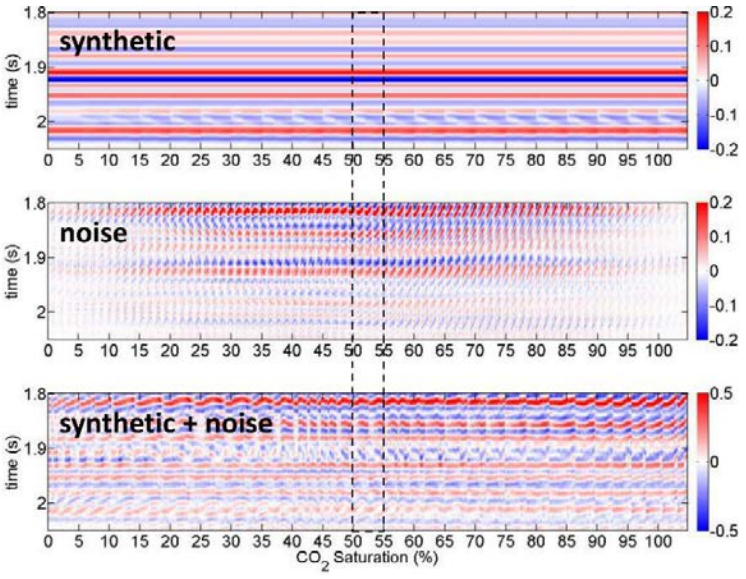

Fig. 4. Showing the (top) synthetic monitor traces (CO_2 saturation of 100%), (middle) noise traces and (bottom) the sum of the monitor and noise traces within the reservoir region (outlined in Fig. 3 by blue dotted box). The black dash lined demarks the synthetic traces for thickness increasing from 1m to 100% of the thickness of the zone at 50% CO_2 saturation.

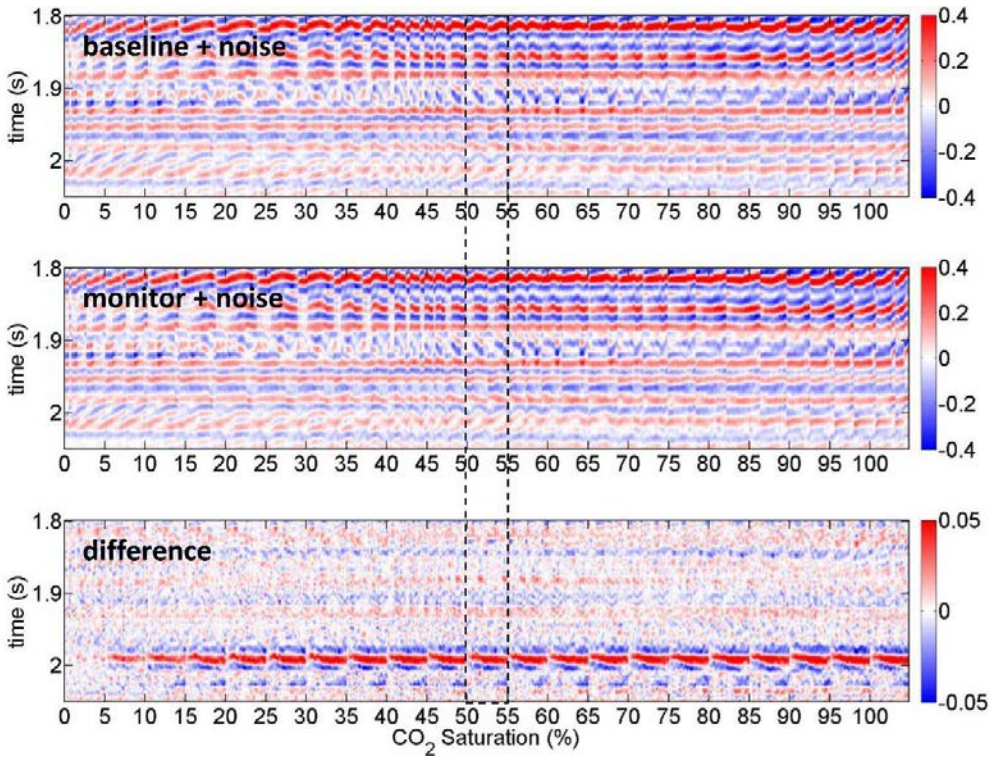

Fig. 5. An example of the amplitude differences between the noisy baseline (top) and noisy synthetic traces (middle; at 100% CO_2 saturation) within the reservoir region for zone 3 as a function of layer thickness and CO_2 saturation (bottom). The black dotted line outlines the amplitude difference for a single CO_2 saturation (50%) where the layer thickness increases from left to right within the outlined section.

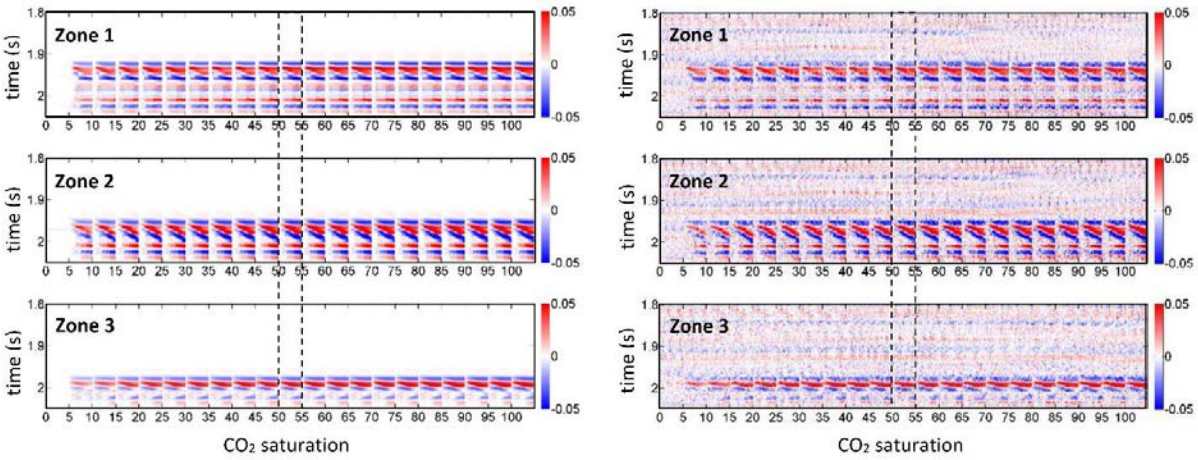

Fig. 6. The amplitude differences between (left) the noise-free baseline synthetic traces and the noise-free monitor synthetic traces, and (right) noisy baseline traces and noisy monitor traces for each zone as a function of layer thickness and CO_2 saturation. The black dotted line outlines the amplitude difference for a single CO_2 saturation (50%) where the layer thickness increases from left to right within the outlined section.

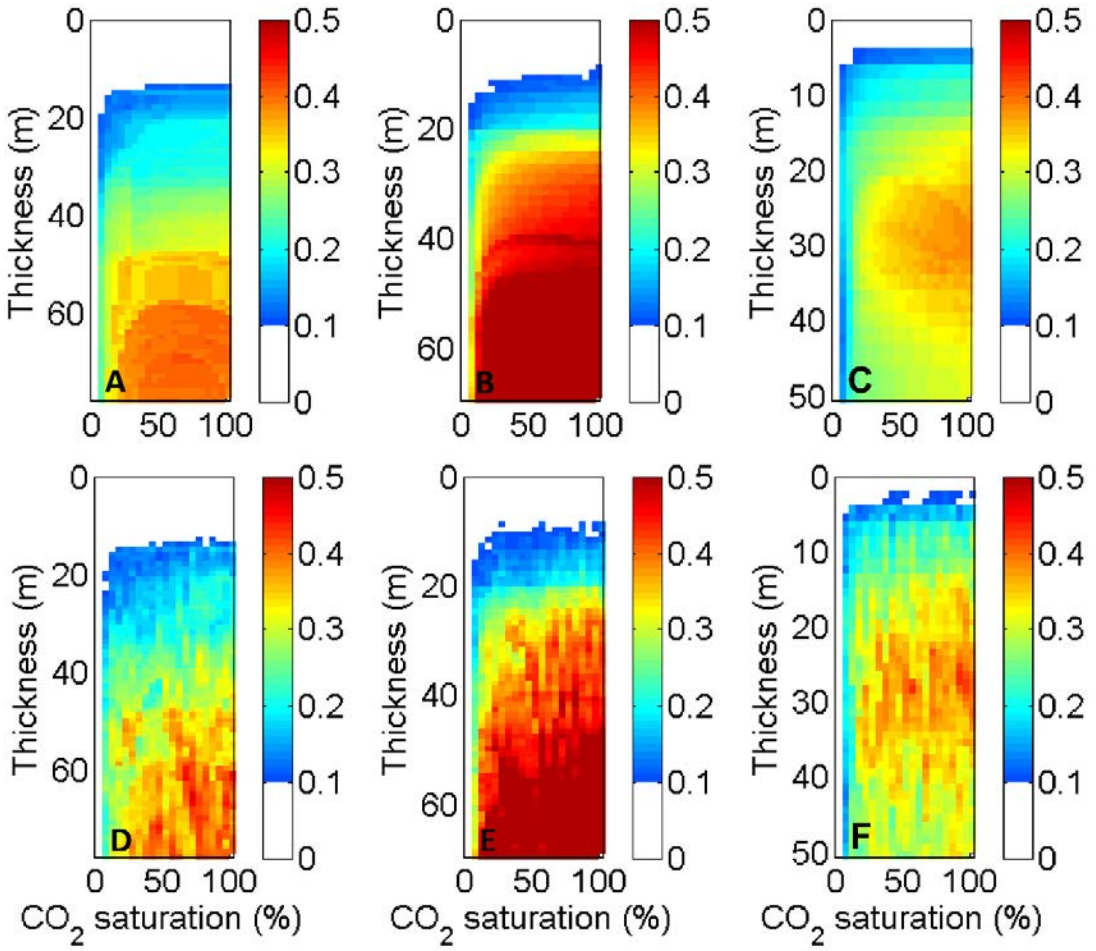

Fig. 7. Maps showing the nRMS between the synthetic baseline and monitor traces as a function of layer thickness and CO_2 saturation. (A to C) for noise-free traces and (D to F) for noisy traces. Each pixel corresponds to a single CO_2 saturation-layer thickness combination. Layer thickness varies in 1 m increments up to 100% of zone thickness and CO_2 saturation varies in 5% increments up to 100%. (A and D) Zone 1: Winnipeg Black Island to Deadwood units, (B and E) Zone 2: Deadwood 1 unit, and (C and F) Zone 3: Deadwood unit. Conditions under which the nRMS is less than 0.1 are masked with white.

5.2. The single-zone models

Fig. 8 through 11 summarise the results of the single-layer reservoir models. Fig. 8 shows an example of the stacks of the synthetic traces with 0% CO_2 saturation, the raw baseline noise traces, and the baseline synthetic traces with the raw baseline noise added at the 'raw' processing stage. Fig. 9 shows the resulting amplitude differences between the 0% CO_2 saturation synthetic (baseline) and the 20% CO_2 saturation synthetic (monitor) traces; the cross-equalised monitor noise and migrated baseline traces; and the cross-equalised noisy 20% CO_2 saturation synthetic and the migrated 0% CO_2 saturation synthetic traces.

The nRMS was computed within a 40ms around the reservoir region on the noise-free synthetic stacks to determine the variation in global nRMS with saturation (Fig. 10). As expected, the global nRMS increases with increasing CO_2 saturation. There is a steep rise in the global nRMS value between the baseline values of 0 to the 20% CO_2 saturation value at 0.08. Over 20% CO_2 saturation, the change in global nRMS decreases. In fact, the difference in the global nRMS between the 20% synthetic and the 50% synthetic is 0.01 and the difference between the 20% synthetic and the 100% synthetic is 0.02.

Fig. 11 displays the variation in nRMS, as a function of processing step, of the noise traces and the synthetics with noise added (20% and 100% CO_2 saturation) for a 40 ms window around the reservoir. Each processing step applied decreases the global nRMS for all datasets indicating that processing flow increases the similarity between the traces with each step – the same observation made with the full 3D datasets in Roach et al. 2015 [12].

For the noise volumes and the noisy synthetic volumes, the best global nRMS result at the reservoir is obtained at the final cross-equalisation step (PTSN) and the characteristic of the curves is similar. The global nRMS of the noise dataset is larger than that of the noisy synthetic datasets up to migration. Following migration, the global nRMS for the noisy synthetic datasets are above that of the noise. The differences in global nRMS between the 20% CO_2 saturation noisy dataset and the 100% CO_2 saturation noisy dataset are insignificant while the difference between the noise dataset and the noisy synthetic datasets is ~0.02, regardless of the stage of processing. These results suggest that when CO_2 replaces brine in the reservoir, its presence can be detected using the global nRMS as a metric if the saturation is above 20%. However, in this particular simulation, the global nRMS cannot distinguish between the CO_2 saturation.

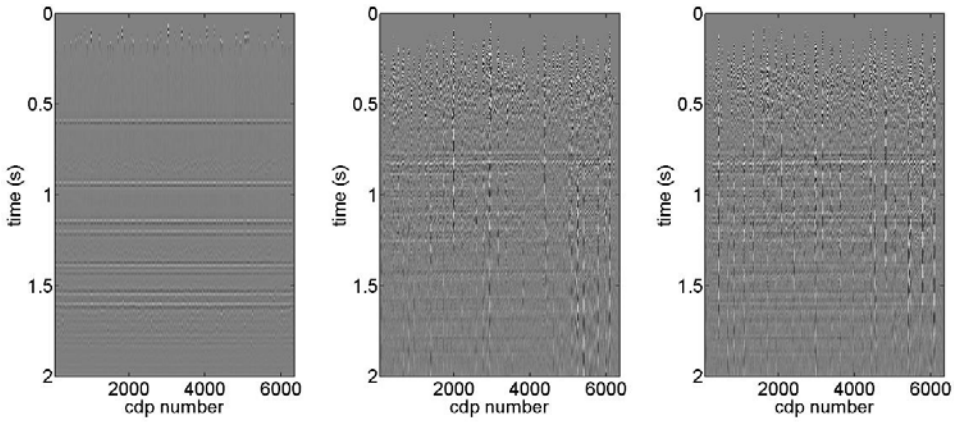

Fig. 8. Stacked traces for all CDPs in data volume. (Left) noise-free baseline synthetic volume, (middle) raw baseline noise volume, and (right) sum the noise-free baseline synthetic and raw baseline noise traces (i.e the sum of the image on the left with the image in the middle).

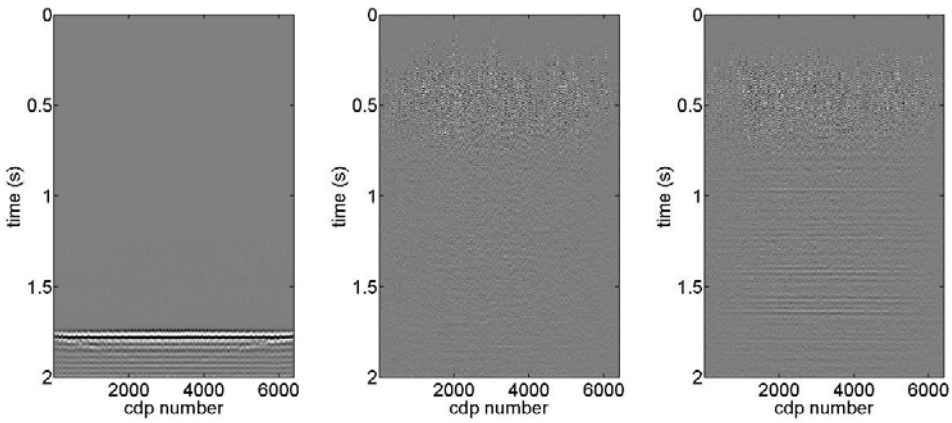

Fig. 9. Amplitude differences for noise-free synthetic (0% minus 20% CO_2 saturation) volumes (left), cross-equalised monitor noise and migrated baseline noise volumes(middle), and cross equalised noisy monitor synthetic data (20% CO_2 saturation) and migrated noisy baseline synthetic (0% CO_2 saturation) volumes(right).

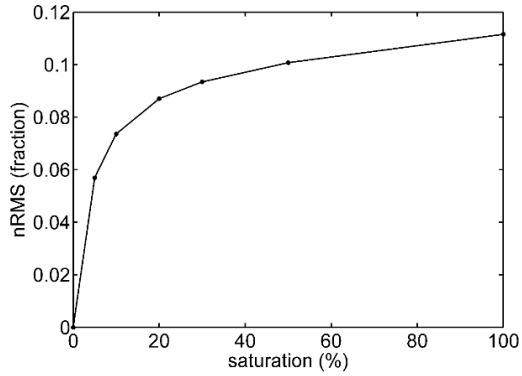

Fig. 10. Variation of global nRMS as a funciton of CO_2 saturation computed for a 40ms window around the reservoir.

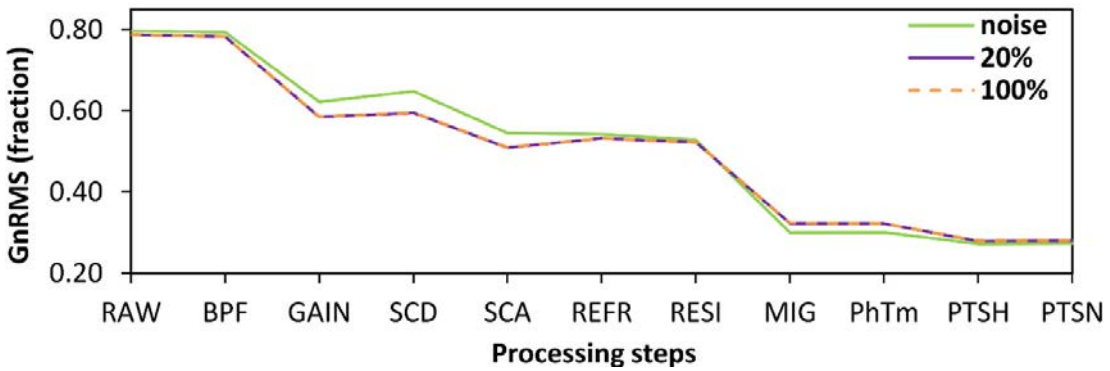

Fig. 11. Global nRMS as a function of processing step for the noise data volumes and 2 noisy monitor volumes – 20% CO_2 saturation and 100% CO_2 saturation. Raw – raw; BPF – bandpass filter applied; GAIN – t^2 gain applied; SCD – surface consistent deconvolution; SCA – surface conssitent Amplitudes; REFR – refraction statics applied; RESI – residual statics applied; MIG – post-stack migration; PhTM – phase-time matching; PTSH – Shape filtering; PTSH – Amplitude normalisation. See [12] for details.

6. Conclusions

The analysis of the global nRMS for two different synthetic datasets with real noise added suggests that: (i) with the thin layers, CO_2 is detectable in all zones under noise conditions provided that at least 5m of the aquifer in each zone is saturated with 5% CO_2; (ii) it is possible to detect the CO_2 using a time-lapse analysis providing that the CO_2 saturation is above 20% for the 193m-thick full saturated layer; and (iii) it is not possible to distinguish between the various CO_2 saturation using the nRMS as a metric when noise is added to the synthetic dataset and analysed.

Acknowledgements

This research was funded by the EPSRC Geological Storage consortium DiSECCS (EP/K035878/1) and EPSRC Early Career Fellowship (EP/K021869/1) held by DA and the EPSRC. We would like to thank the Petroleum Technology Research Centre (PTRC) for access to Aquistore Data. Aquistore is an independent research and monitoring project managed by the PTRC which intends to demonstrate that storing liquid carbon dioxide (CO_2) deep underground (in a brine and sandstone water formation), is a safe, workable solution to reduce greenhouse gases (GHGs).”

References

[1] Eiken O, Ringrose P, Hermanrud C, Nazarian B, Torp TA, Høier L. Lessons learned from 14 years of CCS operations: Sleipner, In Salah and Snøhvit. Energy Procedia 2011; 4: 5541–5548. doi: 101016/jegypro201102541
[2] Ivandic M, Yang C, Lüth S, Cosma C, Juhlin C.Time-lapse analysis of sparse 3D seismic data from the CO2 storage pilot site at Ketzin, Germany. Journal of Applied Geophysics 2012; 84:14-28.doi: 101016/jjappgeo201205010
[3] Sakai A. Monitoring of the carbon dioxide sequestration by time-lapse 3D seismic survey in Japan. In: Rubin ES, Keith DW, Gilboy CF, Wilson M, Morris T, Gale J, Thambimuthu K, editors. Greenhouse Gas Control Technologies; 2005; 7:1253-1258.
[4] White D, 2013, Seismic characterization and time-lapse imaging during seven years of CO2 flood in the Weyburn field, Saskatchewan, Canada. International Journal of Greenhouse Gas Control 2013; 16: S78–S94. doi: http://dxdoiorg/101016/jijggc201302006
[5] Lumley DE. 4D seismic monitoring of CO2 sequestration. The Leading Edge 2010; 29: 150-155. doi:101190/13304817
[6] Biot MA. General theory of three-dimensional consolidation. J. Appl. Phys 1941; 12 (2):155–164. http://dx.doi.org/10.1063/1.1712886
[7] Gassmann F. Über die elastizität poröser medien: Vierteljahrss-chrift der Naturforschenden Gesellschaft in Zurich 1951; 96: 1-23. The English translation of this paper is available at http://sepwwwstanfordedu/sep/berryman/ PS/gassmannpdf.
[8] Kragh E, Christie P. Seismic repeatability, normalized rms, and predictability: The Leading Edge 2002; 21: 640-647.doi: 101190/11497316.
[9] Castagna JP, Batzle ML, Eastwood R L. Relationships between compressional-wave and shear-wave velocities in clastic silicate rocks. Geophysics 1985; 50(4): p571-581.
[10] Batzle M, Wang Z. Seismic properties of pore fluids. Geophysics 1992; 57(11):1396-1408.
[11] Xu Y. Analysis of P-wave seismic response for fracture detection: modelling and case studies PhD thesis University of Edinburgh 2012.
[12] Roach LAN, White DJ, Roberts B. Assessment of 4D seismic repeatability and CO2 detection limits using a sparse permanent land array at the Aquistore CO2 storage site. GEOPHYSICS 2015; 80(2): WA1-WA13 doi:101190/geo2014-02011.
[13] White DJ, Roach LAN, Roberts B. Time-lapse seismic performance of a sparse permanent array: Experience from the Aquistore CO2 storage site: GEOPHYSICS 2015; 80(2): WA35-WA48. doi: 101190/geo2014-02391.